

Contents lists available at ScienceDirect

Journal of Advanced Research

journal homepage: www.elsevier.com/locate/jare



Original Manuscript

CHMP4C promotes pancreatic cancer progression by inhibiting necroptosis via the RIPK1/RIPK3/MLKL pathway



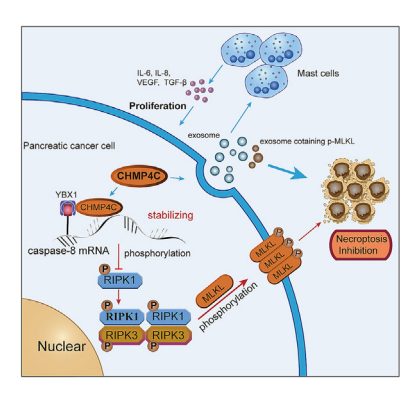
Longchen Yu ^{a,b,1}, Qining Guo ^{a,b,1}, Yaping Li ^{a,b}, Mai Mao ^{a,b}, Zhenping Liu ^{a,b}, Tingting Li ^{a,b}, Lei Wang ^{c,*}, Xin Zhang ^{a,b,*}

- ^a Department of Clinical Laboratory, Qilu Hospital of Shandong University, Jinan 250012 China
- ^b Shandong Engineering Research Center of Biomarker and Artificial Intelligence Application, Jinan 250012 China
- ^c Department of Orthodontics, Qilu Hospital of Shandong University, Jinan 250012 China

HIGHLIGHTS

- CHMP4C promotes pancreatic cancer progression through inhibiting necroptosis and serves as a prognostic predictor for pancreatic cancer.
- CHMP4C interacts with YBX1 to stabilize caspase-8 mRNA, and inhibits the RIPK1/RIPK3/MLKL pathway.
- CHMP4C mediates the excretion of p-MLKL via extracellular vesicles.

GRAPHICAL ABSTRACT



ARTICLE INFO

Article history: Received 16 October 2024 Revised 10 January 2025 Accepted 24 January 2025 Available online 25 January 2025

Keywords: CHMP4C Pancreatic cancer Necroptosis Extracellular vesicles Biomarker

ABSTRACT

Introduction: Pancreatic cancer (PC) cannot currently be completely cured and has a poor prognosis. Necroptosis is a distinct form of regulated cell death that differs from both necrosis and apoptosis. Understanding the role of necroptosis during PC progression would open new avenues for targeted therapy.

Objectives: The purpose of this study is to examine the impact of necroptosis on the progression of PC and related mechanisms.

Methods: RNA sequencing was performed to identify necroptosis-related genes that are differentially expressed in PC tissues. The biological functions of CHMP4C and its necroptosis effects were determined in vitro and in vivo. RNA immunoprecipitation, MeRIP-qPCR, Co-immunoprecipitation assays were conducted to evaluate the interaction among CHMP4C, YBX1 and caspase-8 mRNA. Extracellular vesicles were isolated using the differential ultracentrifugation method. The expression of CHMP4C, p-MLKL and CD117 were detected on a PC tissue microarray using multiplex immunofluorescence staining. Results: CHMP4C was significantly overexpressed in PC cells and tissues. It promoted cell growth and suppressed necroptosis of PC cells in both in vivo and in vitro settings. Mechanistically, CHMP4C interacted with YBX1 to mediate m⁵C modification of caspase-8 mRNA, resulting in increased caspase-8 expression and inhibition of RIPK1/RIPK3/MLKL pathway phosphorylation. Furthermore, CHMP4C

^{*} Corresponding authors at: Qilu Hospital of Shandong University, Jinan 250012, China (Lei Wang and Xin Zhang). E-mail addresses: dentistwl@126.com (L. Wang), xinzhang@sdu.edu.cn (X. Zhang).

 $^{^{1}\,}$ The authors share equal contributions to this research.

promoted extracellular exocytosis of p-MLKL to further suppress necroptosis. Additionally, PC cells used CHMP4C within extracellular vesicles to recruit and stimulate mast cells (MCs), which in turn promoted PC cell proliferation. In PC tissues, the expression of CHMP4C showed a negative correlation with p-MLKL and a positive association with CD117. High expression levels of CHMP4C in patients were associated with poorer overall survival outcomes.

Conclusions: CHMP4C promotes PC progression by inhibiting necroptosis, which has potential as a biomarker and therapeutic target in PC.

© 2025 Published by Elsevier B.V. on behalf of Cairo University. This is an open access article under the CC BY-NC-ND license (http://creativecommons.org/licenses/by-nc-nd/4.0/).

Introduction

Pancreatic cancer (PC) ranks as the third most common cause of cancer-related deaths globally, with a five-year survival rate less of than 10 % [1,2]. Early-stage PC is often undiagnosed until it has advanced, with up to 85 % of patients experiencing recurrences after surgery, resulting in a poor prognosis [3,4]. Modified FOLFIR-INOX (fluorouracil, oxaliplatin, irinotecan, and leucovorin) is a recommended postoperative chemotherapy treatment that improves survival in advanced PC by inducing apoptosis [5]. However, chemoresistance resulting from tumor cells evading apoptosis remains a major issue, necessitating new therapeutic strategies [6]. Implementing cancer therapies that target alternative forms of cell death beyond apoptosis presents a promising avenue for overcoming chemoresistance.

Necroptosis is programmed necrosis, a specific form of programmed cell death that differs from both apoptosis and necrosis [7]. During necroptosis, the phosphorylation of signaling pathway involving receptor interacting protein kinase 1 and 3 (RIPK1 and RIPK3) activates the mixed lineage kinase domain-like (MLKL) kinase, resulting in cell swelling and rupture of the membrane [8]. An increasing number of research have reported that necroptosis plays a significant role in the occurrence and progression of various malignancies, such as PC [9,10]. For example, Zhao and colleagues [11] identified that the pyridazinone compound IMB5036 enhanced the level of phosphorylated RIPK1, RIPK3, and MLKL in PC cells, leading to necroptosis and suppression of tumor cell proliferation. Moreover, necroptosis can trigger the secretion of SAP130 from PC cells, which interacts with its receptor Mincle to create an immunosuppressive tumor microenvironment, thereby facilitating PC progression [12]. Two studies have demonstrated that PC patients with high-risk scores defined by necroptosis-related prognostic models had poor survivals [13,14]. However, the mechanisms regulating necroptosis in PC remain inadequately understood.

Extracellular vesicles (EVs) are secreted into the extracellular environment after multivesicular bodies (MVBs) fuse with the plasma membrane and are released by various cell types [15]. EVs can contain a diverse array of biomolecules, such as proteins, lipids and genetic material [16]. Tumor cells have the ability to actively release toxic proteins and tumor suppressors through EVs, resulting in maintained cellular balance and the support of cancer development [17]. Yoon *et al.* [18] demonstrated that RIPK3 promotes the release of EVs containing p-MLKL and the endosomal sorting complex required for transport (ESCRT), which antagonizes p-MLKL mediated necroptosis. Similarly, the exocytosis of p-MLKL via EVs was reported to reduce necroptosis induction by PCB29-pQ [19]. Consequently, EVs are implicated in the modulation of necroptosis.

Chromatin Modification Protein 4C (CHMP4C) belongs to the charged multivesicular body protein family and participates in the assembly of ESCRT-III, which is crucial for endosomal trafficking and mitosis [20]. Recent studies have reported that CHMP4C was implicated in the regulation of some cancers progression and chemoresistance [21–23]. Specifically, p53-mediated upregulation

of CHMP4C is necessary for increased EVs release, and inhibiting CHMP4C reduced EVs release in lung cancer cells [24]. Our previous study observed that CHMP4C, a component of a necroptosis-related prognostic signature, was significantly elevated in both tumor tissues and serum EVs of PC patients. However, until now, the role of CHMP4C in PC and its impact on necroptosis have not been studied.

This study systematically examined the involvement of CHMP4C in the tumorigenesis and progression of PC. Our findings reveal an increase in CHMP4C expression in PC tissues, which facilitated the growth of PC cells. Furthermore, CHMP4C suppressed necroptosis in PC cells by inhibiting the phosphorylation of the RIPK1/RIPK3/MLKL signaling pathway and promoting the extracellular secretion of p-MLKL. The upregulation of CHMP4C is indicative of PC advancement and may act as a promising therapeutic target and biomarker for PC.

Materials and methods

Cell culture and treatment

The human normal pancreatic ductal epithelial cell line (HPDE6-C7), PC cell lines (PANC-1 and BxPC3), and the human mast cell line (HMC-1) were purchased from the Type Culture Collection of the Chinese Academy of Sciences. All cells were maintained in DMEM (Gibco-BRL) medium supplemented with 10 % fetal bovine serum (FBS, Gibco) and 1 % penicillin or streptomycin (Gibco). All cell lines were grown at 37 °C in a 5 % CO₂ cell culture incubator. The conditioned medium (CM) of HMC-1 cells was collected and diluted to 1/3 with DMEM medium prior to its utilization [25]. The necroptosis inducers employed in this study include TNFa, Smac mimics, and zVAD-FMK (TSZ, C1058S, Beyotime). The inhibitors used in this study are Necrostatin-1 (Nec-1, S8037, Selleck Chemicals), an inhibitor of necroptosis; Ferrostatin-1 (S7243, Selleck Chemicals), an inhibitor of ferroptosis; and Chloroquine (S6999, Selleck Chemicals), an inhibitor of autophagy.

RNA sequencing

All tissues samples were collected from PC patients hospitalized in Qilu Hospital of Shandong University. Total RNAs were extracted using traditional Trizol method. Sequencing libraries were constructed using VAHTS Universal V8 RNA-seq Library Prep Kit for Illumina (Vazyme, Nanjing, China) as previously described [26]. High-throughput sequencing was conducted using a NovaSeq 6000 sequencer (Illumina, San Diego, CA, USA) and the sequencing data were uploaded to the CNSA database (https://db.cngb.org/cnsa, accession number CNP0006218).

Cell transfection

The lentiviruses for CHMP4C overexpression (OE-CHMP4C) and knockdown (Sh-CHMP4C) were designed by OBIO (Shanghai,

China) and transfected into PANC-1 and BxPC3 cells. The screening of stably transfected cell lines was conducted using 5 μ g/ml puromycin. SiRNAs targeting YBX1 and plasmid for YBX1 were constructed by Genepharma (Shanghai, China), and transiently transfected into PANC-1 and BxPC3 cells using the Lipofectamine 3000 kit (Invitrogen, USA). The sequences targeted by shRNAs and siRNAs are provided in **Supplemental Table 1**.

RT-qPCR

Total RNA was extracted from HPDE6-C7, PC and HMC-1 cell lines using TRIzol reagent (Vazyme) following the instructions. RNA was reverse transcribed into cDNA using the HiScript III 1st-Strand cDNA Synthesis Kit (Vazyme), and then amplified using the QuantiTect SYBR Green PCR Kit (Vazyme) in a QuantStudio 5 Flex Real-Time PCR System (Thermo Fisher Scientific, USA) [27]. The relative expression was determined by the $2^{-\Delta\Delta CT}$ method, with GAPDH serving as the internal control gene. The PCR primers using for each mRNA were designed by BioSune Biotechnology (Shanghai, China) and are presented in **Supplemental Table 2**.

Cell Counting Kit-8 (CCK8) assay and colony formation assay

For the CCK8 assay, stably transfected PANC-1 or BxPC3 cells were plated into 96-well plates at the density of 3×10^3 cells per well and allowed to proliferate for 0, 1, 2, 3, and 4 days, before 10 μ L of the CCK-8 reagent (Abbkine, Wuhan, China) was added per well prior to incubation for 2 h at 37 °C. The absorbance at 450 nm was recorded using a Bio-Rad microplate reader (USA). For the colony formation assay, 1×10^3 stably transfected PANC-1 or BxPC3 cells were plated into six-well plates and incubated for two weeks at 37 °C with 5 % CO2. Colonies were fixed with 4 % paraformaldehyde, stained using a 0.1 % crystal violet solution, and subsequently photographed and counted.

Migration assay

Twenty-four-well plates with uncoated transwell inserts (Corning, USA) were utilized to perform the MCs migration assay. Therein, 700 μl of DMEM medium with 10 % FBS or CM of stably transfected PANC-1 cells were added to each lower chamber, and 1 \times 10 5 HMC-1 cells were added to each upper chamber. Twenty-four hours later, the inserts were treated with 4 % paraformaldehyde for fixation and subsequently stained with crystal violet. Migrated cells were photographed by an inverted optical microscope (Olympus, Japan) and counted using Image J software (version 1.54).

Mouse xenograft model

Stably transfected PANC-1 cells were injected subcutaneously into the armpit region of four-week-old male BALB/c nude mice. Each group contained six mice. After 1 week, mice were injected subcutaneously with Nec-1 (1.65 mg/Kg), and controls were injected with an equal amount of DMSO, 3 times per week [28]. Tumors were assessed every three days, and their volumes were calculated using the equation: volume = $0.52 \times \text{length} \times \text{width}^2$ [29]. After approximately 24 days, the nude mice were culled and subcutaneous xenografts were obtained.

Immunohistochemistry (IHC)

The tumor tissues were preserved in paraformaldehyde and subsequently embedded in paraffin. Endogenous peroxidase activity was inactivated by the addition of 3 % hydrogen peroxide. The sections were incubated overnight at 4 °C after being blocked with

10 % goat serum and treated with primary antibodies. The sections were incubated at room temperature for one hour with a horseradish peroxidase-conjugated secondary antibody. The activities were detected using a DAB kit (Solarbio, Beijing, China), and the nuclei were counterstained with hematoxylin. Primary antibodies utilized in the study included anti-CHMP4C (1:200, DF15365, Affinity), anti-Ki67 (1:200, ab15580, Abcam) and anti-p-MLKL (1:250, ab187091, Abcam).

Characterization of necroptosis

PANC-1 and BxPC3 cells were cultured in 6-well plates until 50 % to 60 % confluent, at which point they were treated using distinct methods. Samples were collected after 0.25 % trypsin without EDTA treatment and washed twice with PBS. Staining was conducted for 15 min at 37 °C in the dark using Annexin V-FITC and PI apoptosis detection kits (Vazyme, China) according to the instructions. Next, the cells were measured on a FACScan flow cytometer (Becton Dickinson, USA). The data were analyzed using FlowJO software (Tree Star, USA). Furthermore, the cells were stained with Hoechst33342/PI double staining kit (Bestbio, Shanghai, China) for 15 min at 37 °C in the dark as the manufacturer's guidelines. A fluorescence microscope (Olympus, Japan) was used to observe the fluorescence of experimental cells in each group. Ultrastructural changes in necroptotic cells were examined using transmission electron microscopy (TEM).

Western blotting assay

Proteins were extracted from PANC-1, BxPC3 and HMC-1 cells, using RIPA lysis buffer (Beyotime, China), and protein concentrations were determined using the BCA Protein Quantification Kit (Abbkine, China). Proteins were subjected to separation via 10 % SDS-PAGE, followed by transfer onto PVDF membranes. The membranes were incubated in a blocking solution of 5 % skim milk for 1 h, followed by an overnight incubation with primary antibodies at 4 °C, and then treated with HRP-conjugated secondary antibodies at room temperature for 1 h. The antibodies used were as follows: anti-CHMP4C (1:1000, DF15365, Affinity), anti-RIPK1 (1:1000, ab300617, Abcam), anti-MLKL (1:1000, ab184718, ABclonal), anti-p-RIPK1 (1:1000, ab316923, ABclonal), anti-p-RIPK3 (1:1000, ab255705, ABclonal), anti-p-MLKL (1:1000, ab187091, Abcam), anti-caspase-8 (1:1000, A0215, ABclonal), anti-IL-6 (1:1000, ab233706, Abcam), anti-CCL2 (1:1000, A23288, ABclonal), anti-SCF (1:1000, A5672, ABclonal), anti-VEGFA (1:1000, ab46154, Abcam), anti-RIPK3 (1:1000, ab316957, ABclonal), anti-TGF-β (1:1000, ab215715, Abcam), anti-Alix (1:1000, ab275377, Abcam), anti-CCL5 (1:1000, A5630, ABclonal), anti-TSG101 (1:1000, ab125011, Abcam), anti-IL-8 (1:1000, ab289967, Abcam), anti-CD63 (1:1000, ab134045, Abcam), anti-YBX1 (1:1000, ET1609-10, HuaBio), and anti-Calnexin (1:1000, ab22595, Abcam).

RNA half-life assay

PANC-1 and BxPC3 cells that were stably transfected were plated in 12-well plates. When the degree of fusion reached 70–80 %, 5 μ g/ml actinomycin D (Aladdin, China) was added, and cell samples were collected at 0, 1, 2, 3, 4, and 5 h post-treatment. Total RNA was isolated using RNA-easy Isolation Reagent (Vazyme, China) and subjected to RT-qPCR analysis.

RNA immunoprecipitation (RIP) and MeRIP-qPCR assay

The RIP assay was performed on PANC-1 and BxPC3 cells by an RNA Immunoprecipitation Kit (Geneseed Biotech, Guangzhou, China) as preciously described [30]. A mixture containing RNA

and protein was obtained and incubated with anti-CHMP4C, anti-YBX1, and anti-IgG antibodies along with magnetic beads. RNA was then isolated using an adsorption column and analyzed via RT-qPCR. MeRIP assays were conducted with an $\rm m^5C$ MeRIP Kit (BersinBio, Guangzhou, China) as preciously described [31]. Cellular RNA was extracted and the RNA sample was fragmented into approximately 100 nt fragments. Immunoprecipitation was performed by the addition of 4 $\rm \mu g$ of IgG or $\rm m^5C$ antibody at 4 °C. Subsequently, protein A/G magnetic beads were utilized to bind the antibody. After washing the magnetic beads, the precipitated RNA was eluted for RT-qPCR analysis.

Co-immunoprecipitation (CO-IP) assay

Co-IP assays were conducted on PANC-1 cells using the Universal IP/Co-IP Toolkit (Abbkine, Wuhan, China) as preciously described [32]. The mixture of magnetic beads and antibody was mixed at 37 $^{\circ}$ C for 30 min. Then, the collected cell lysates were added to magnetic beads and mixed overnight at 4 $^{\circ}$ C to form immunoprecipitated protein complexes. The magnetic bead complexes were washed with lysis buffer and then the bound proteins were subsequently eluted for further analysis through western blotting and mass spectrometry (MS) identification.

Evs isolation and phagocytosis assays

Evs were obtained from PANC-1 cell-conditioned medium through differential ultracentrifugation as previously described [33]. Evs were imaged by TEM and their size were analyzed by nanoparticle tracking analysis (NTA). The presence of EV biomarkers (Alix, TSG101, and CD63) was assessed using western blotting. To monitor Evs trafficking, Evs were labeled using a PKH67 Red Fluorescent Cell Linker Kit (Solarbio, Beijing, China).

Multiplex immunofluorescence staining of tissue microarray

Tissue microarrays consisting of formalin-fixed, paraffinembedded sections from pancreatic ductal adenocarcinoma (PAAD) tissues were obtained from Shanghai Outdo Biotech (Superchip, China). Multiplex immunohistochemistry was conducted through multiple staining rounds, starting with a protein block using 1 % BSA, followed by incubation with primary antibodies and corresponding horseradish peroxidase-conjugated secondary antibodies targeting mouse or rabbit immunoglobulins (Akoya Biosciences). Subsequently, the slides underwent incubation with different Opal fluorophores (1:100), prepared in $1 \times Plus$ Amplification Diluent (Akoya Biosciences). The following primary antibodies were employed: anti-CD117 (1:250, ab283653, Abcam), anti-p-MLKL (1:200, ab187091, Abcam), and anti-CHMP4C (1:200, DF15365, Affinity). The slides were stained with spectral DAPI (Akoya Biosciences) for nuclear visualization and mounted using Anti-fade fluorescence mounting medium (ab104135, Abcam). Images were scanned using a slide scanner (PANNORAMIC SCAN II Imaging System). Cell segmentation was performed using an algorithm based on DAPI staining of cell nuclei. Intensity of cellular fluorescent staining for each marker was measured using QuPath V.0.4.3 (Queen's University). The clinical samples and corresponding data utilized in this research were approved by the Shanghai Outdo Biotech Company's Ethics Committee.

Bioinformatics analysis

The gene expression profiles for PAAD samples and paired normal tissues from TCGA and GTEx databases were obtained from GEPIA2 (https://gepia2.cancer-pku.cn/). Additional PAAD datasets

were retrieved from publicly accessible GEO databases, including GSE183795 and GSE85916. The Gene Set Enrichment Analysis (GSEA) was conducted on the normalized data using the GSEA_4.3.0 software.

Statistical analysis

To evaluate the data distribution from in vitro and in vivo experiments, the Kolmogorov-Smirnov test was utilized. In cases where the distribution was normal, the student's *t*-test was conducted for two-group comparisons, and one-way ANOVA was used for comparisons among multiple groups. Otherwise, we used the Mann-Whitney U test for two-group comparisons and the Kruskal-Wallis test for multiple-group comparisons. Additional post-hoc multiple group comparisons were conducted using Dunn's Test. The figure legends provide further details on the specific tests employed. Relationship between CHMP4C expressions and clinicopathological parameters was estimated by $\chi 2$ test. Correlations between CHMP4C and caspase-8, p-MLKL, or CD117 were calculated using Pearson's analysis. Overall survival (OS) was evaluated using the Kaplan-Meier method in conjunction with the log-rank test. Statistical analysis were conducted by IBM SPSS Statistics (version 26), GraphPad Prism (version 8.0) software or RStudio (version 4.2.1), and p-value of less than 0.05 was considered to be statistically significant.

Results

CHMP4C is upregulated in PC tissues and facilitates tumorigenesis

To analyze the differentially expressed genes in PC, RNA sequencing was conducted on five pairs of PC tissues and adjacent normal tissues. A total of 2872 mRNAs were identified (|Log2FC| > 1, P. adj < 0.05), including 1597 upregulated and 1275 downregulated (Fig. 1A). Based on these genes, KEGG analysis revealed necroptosis was one of the most significant pathways (Fig. 1B and Supplemental Table 3). Furthermore, Heatmap showed PC tissues were well distinguished from adjacent normal tissues based on 39 differentially expressed necroptosis-associated genes (Fig. 1C). Among them, CHMP4C was identified as being significantly overexpressed in PAAD tissues from external databases, such as TCGA and GSE21501 datasets (Supplemental Fig. S1A and B). RT-qPCR and western blotting assays confirmed the levels of CHMP4C were increased in the above five tumor tissues (Fig. 1D and E).

Compared to normal pancreatic ductal epithelial cell line (HPDE6-C7), CHMP4C was also more highly expressed in PC cells (PANC-1 and BxPC3) (Fig. 1F). Subsequently, we established CHMP4C silenced or overexpressed cell lines by lentiviral transfection (Supplemental Fig. S1C and D). As shown in Fig. 1G and H, overexpression of CHMP4C promoted the proliferation of PC cells, while CHMP4C knockdown inhibited their growth, as revealed by CCK8 and clone formation assays.

CHMP4C inhibits necroptosis of PC cells in vitro

To investigate whether CHMP4C is a regulator of necroptosis, TSZ was employed to induce necroptosis in PC cells. The data showed that the upregulation of CHMP4C inhibited TSZ-induced cell death in PANC-1 and BxPC3 cells, while CHMP4C depletion resulted in the opposite effect (Fig. 2A). Observation by TEM revealed that the morphology of cells overexpressing CHMP4C was not significantly altered after TSZ treatment, while TSZ treated control cells underwent obvious necroptotic morphological changes, such as swelling of nuclei, disruption of cell membrane

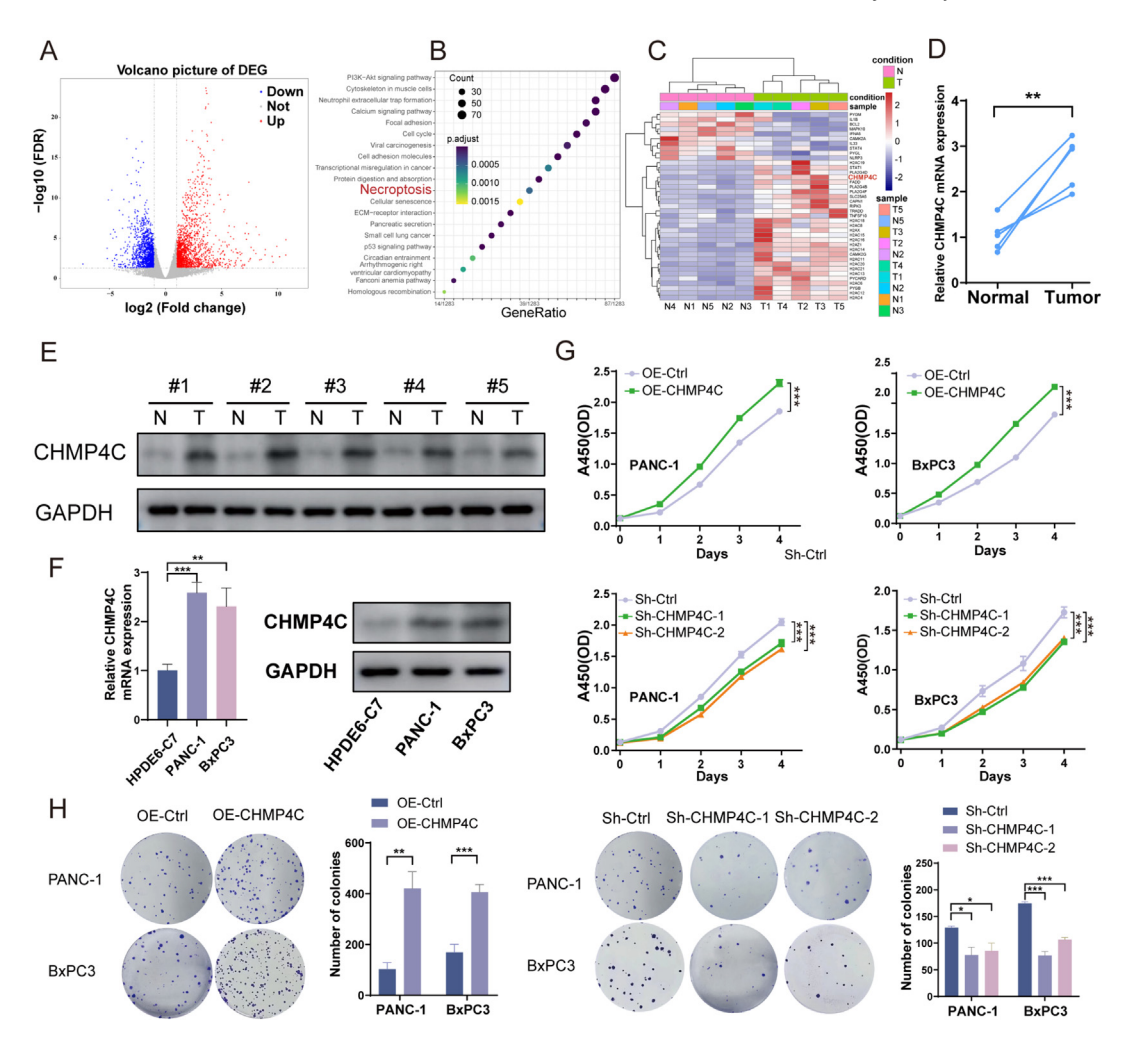


Fig. 1. CHMP4C is upregulated in PC and facilitates tumorigenesis. (**A**) A volcano plot showing the differentially expressed genes in PC tissues. (**B**) KEGG pathway enrichment analysis of PC tissue compared with adjacent normal tissue. (**C**) Heatmap showing differential expression of necroptosis-related genes between PC tissue and adjacent normal tissue. (**D**, **E**) The mRNA and protein level of CHMP4C in 5 paired PAAD tissues and adjacent non-tumor tissues (paired Student *t* test). (**F**) Expression levels of CHMP4C mRNA and protein in HPDE6-C7, PANC-1 and BxPC3 cell lines (one-way ANOVA). (**G**, **H**) CCK8 (**G**) and colony formation assays (**H**) reaveled the effects of CHMP4C on PANC-1 or BxPC3 cell proliferation (one-way ANOVA). **P < 0.05; **P < 0.01; ***P < 0.001. Data are presented as mean ± SD.

integrity, and swelling of mitochondria (Fig. 2B). Flow cytometry and Hoechst 33342/Pl double staining results showed a significant reduction in the proportion of Pl-positive cells in the overexpression group compared to the control group, and both groups exhibited more obvious differences after TSZ treatment (Fig. 2C and D). Western blotting analysis revealed that overexpression of CHMP4C significantly decreased the level of phosphorylation of proteins of the RIPK1-RIPK3-MLKL pathway, whereas knockdown of CHMP4C promoted their phosphorylation (Fig. 2E).

To further validate the above hypothesis, we administered the necroptosis inhibitor Nec-1 to CHMP4C knockdown cells. In CHMP4C-knockdown PC cells, treatment with Nec-1 increased proliferative viability and clone formation (Fig. 3A, B and Supplemental Fig. S2A). TEM results showed that Nec-1 alleviated the altered cell morphology caused by CHMP4C knockdown (Fig. 3C). The increased necroptosis sensitivity in CHMP4C-knockdown PC cells was reversed by necroptosis inhibitor (Nec-1), but not by the ferroptosis inhibitor (ferrostatin-1) or autophagy inhibitor (chloroquine) (Fig. 3D). As such, it suggested that the increased sensitivity to cell death in CHMP4C-knockdown cells is a result of necroptosis. Furthermore, the increased proportion of Plpositive cells was rescued by Nec-1 (Fig. 3E and F, Supplemental Fig. S2B and C). Western blotting analysis revealed that the levels of phosphorylation of RIPK1, RIPK3, and MLKL were significantly

decreased in PANC-1 and BxPC3 cells after Nec-1 treatment (Fig. 3**G**). These results indicate that CHMP4C promoted PC progression by inhibiting the RIPK1-RIPK3-MLKL necroptotic signaling axis.

CHMP4C promotes the growth of pancreatic xenografted tumors and inhibits necroptosis in vivo

To further investigate the hypothesis that CHMP4C promotes PC progression by inhibiting necroptosis, in vivo PANC-1-derived xenograft mouse models were constructed. We observed that overexpression of CHMP4C in PANC-1 cells significantly promoted xenograft tumor growth compared to controls. The weight of the xenograft tumors excised from the overexpression group was significantly higher (Fig. 4A). In contrast, knockdown of CHMP4C significantly inhibited the growth and weight of xenograft tumors (Fig. 4B). Furthermore, subcutaneous injection of Nec-1 significantly alleviated the inhibitory effect of CHMP4C downregulation on tumor growth (Fig. 4C). We further extracted proteins from three tumors in each group and found that upregulation of CHMP4C inhibited the phosphorylation of proteins in the RIPK1-RIPK3-MLKL pathway (Fig. 4D). Furthermore, the phosphorylation levels of RIPK1, RIPK3 and MLKL proteins were elevated in the knockdown group compared to the control group (Fig. 4E), which

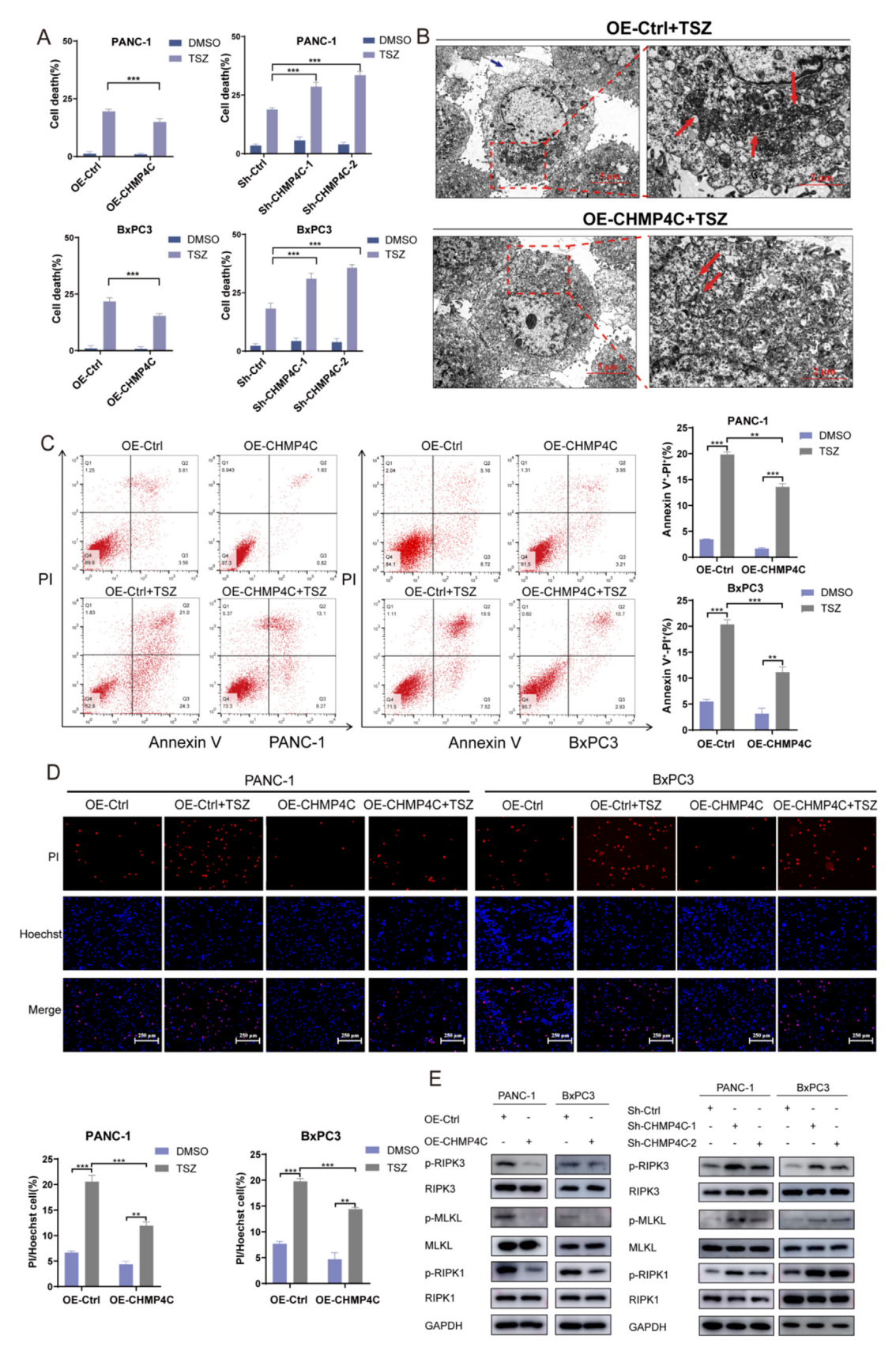


Fig. 2. CHMP4C negatively regulates necroptosis by inhibiting RIPK1/RIPK3/MLKL pathway phosphorylation. (A) Cell viability of stably transfected PANC-1 and BxPC3 cells after treatment with TSZ. (B) TEM images of PANC-1 cells with differentially-expressed CHMP4C protein after treatment with TSZ. The red arrows indicate the mitochondria. (C) The Annexin V and PI-positive cells rate of stably transfected PANC-1/BxPC3 cells with or without TSZ treatment was analyzed by flow cytometry. (D) Hoechst 33342/PI staining showed PI uptake of stably transfected PANC-1/BxPC3 cells with or without TSZ treatment (scale bar = 250 μm). (E) The expressions of RIPK1, RIPK3, MLKL and their phosphorylated proteins in stably transfected PANC-1 or BxPC3 cells were detected by western blotting. one-way ANOVA, *P < 0.05; **P < 0.01: ***P < 0.001. Data are presented as mean ± SD. (For interpretation of the references to colour in this figure legend, the reader is referred to the web version of this article.)

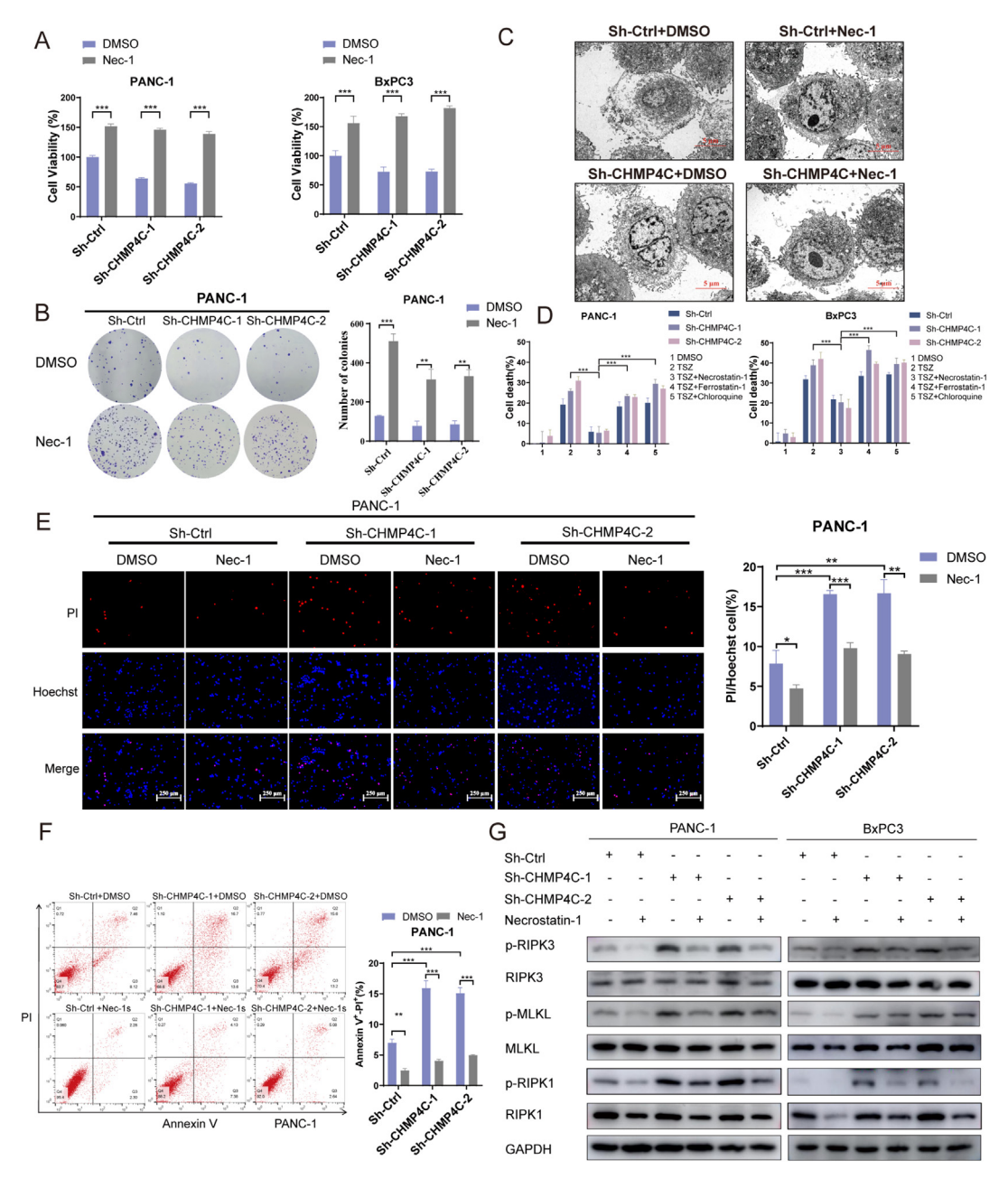


Fig. 3. Nec-1 reverses necroptosis induced by CHMP4C knockdown. CCK8 (A) and Colony formation assays (B) represent the cell viability and proliferation of CHMP4C-knockdown PC cells after Nec-1 treatment. (C) TEM images of CHMP4C-knockdown PC cells after Nec-1 treatment. (D) Cell viability of CHMP4C-knockdown PC cells after treatment with TSZ in the presence or absence of Nec-1(30 μ M), ferrostatin-1 (1 μ M), and chloroquine (20 μ M). (E, F) Indicated cells were analyzed by Hoechst 33342/PI double staining under fluorescence microscope (scale bar = 250 μ m) (E) or quantified by flow cytometer (F). (G) The expressions of RIPK1, RIPK3, MLKL and their phosphorylated proteins in indicated cells were detected by western blotting. *P < 0.05; **P < 0.01; ***P < 0.001. one-way ANOVA, Data are presented as mean ± SD.

is consistent with our previous *in vitro* observations. Moreover, Nec-1 reversed the elevated levels of RIPK1, RIPK3 and MLKL phosphorylation induced by CHMP4C knockdown (Fig. 4F). IHC analysis revealed that CHMP4C downregulation significantly suppressed the level of the tumor proliferation marker Ki67, but increased the expression of p-MLKL (Fig. 4G). Taken together, these findings demonstrate *in vivo* the inhibitory effect of CHMP4C on the RIPK1-RIPK3-MLKL signaling axis that resulted in promotion of PC growth in a xenograft tumor model.

CHMP4C interacts with YBX1 to regulate caspase-8 stabilization in PC cells

It is widely reported that caspase-8 serves as an endogenous inhibitor to block necroptosis through cleaving RIPK1 or inhibiting RIPK1 and RIPK3 phosphorylation [34,35]. To better understand the mechanism by which CHMP4C modulates the phosphorylation of RIPK1, RIPK3, and MLKL proteins, we further investigated the effects of CHMPC4 on caspase-8. A positive correlation between CHMP4C and caspase-8 in PAAD tissues was observed in correlation analysis using GEPIA2 (Fig. 5A). Overexpression of CHMPC4 increased caspase-8 mRNA and protein levels, while knockdown of CHMPC4 had the opposite effect (Fig. 5B, C and Supplemental Fig. S3A). RIP assays with CHMP4C antibodies showed that CHMP4C could bind to caspase-8 mRNA (Fig. 5D and Supplemental Fig. S3B). Given that CHMP4C is mainly localized in the cytoplasm, we further investigated whether CHMP4C regulates caspase-8 expression by affecting the stability of its mRNA. Actinomycin D assays revealed that the stability of caspase-8 mRNA was significantly reduced upon CHMP4C silencing (Fig. 5E and Supple-

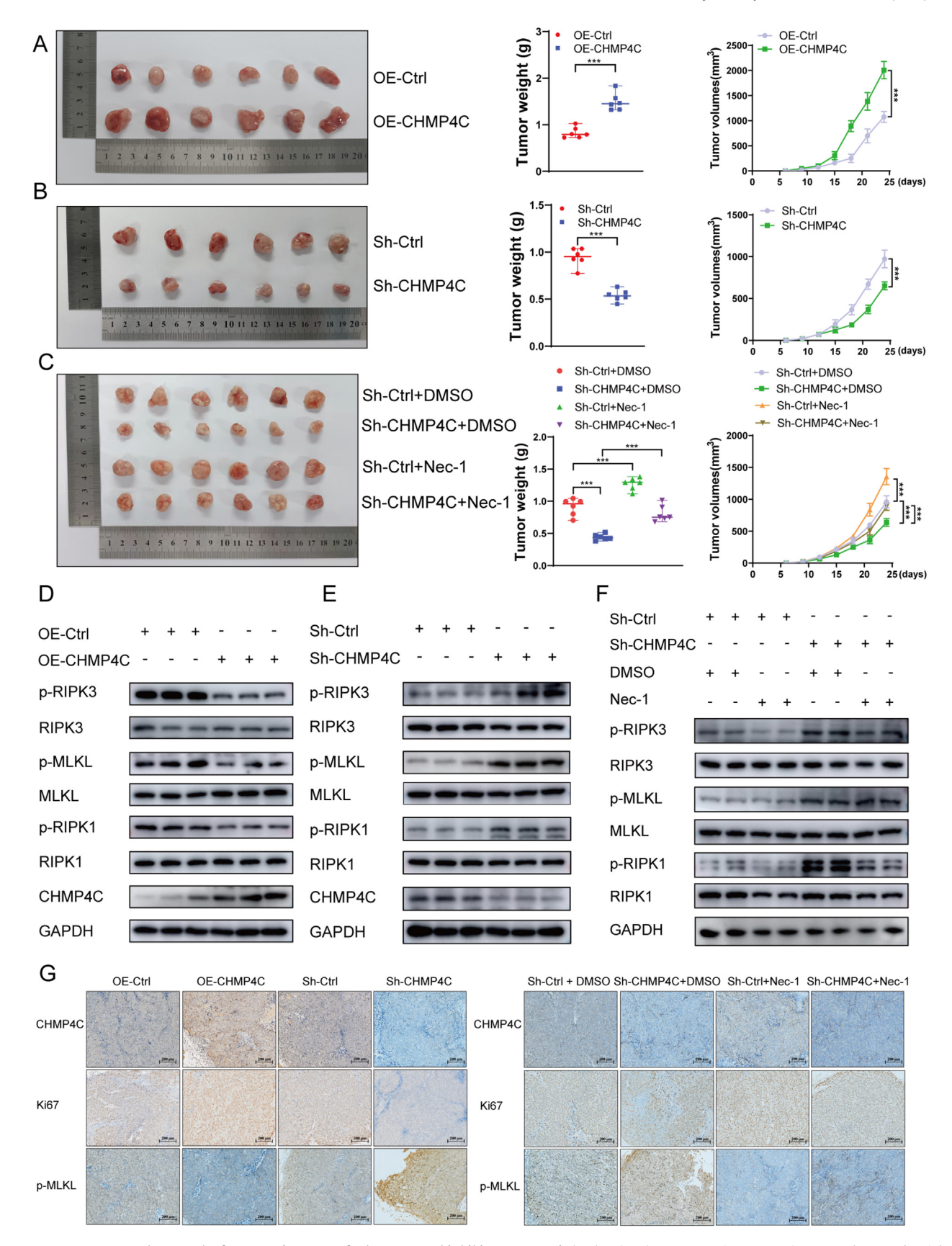


Fig. 4. CHMP4C promotes the growth of pancreatic xenografted tumors and inhibits necroptosis in vivo. (A, B) Representative tumour images, volume and weight from control, CHMP4C-overexpressing and CHMP4C-knockdown PANC-1 xenograft model (Mann-Whitney U test). (C) Representative tumour images, volume and weight of PANC-1 xenograft model in Sh-Ctrl + DMSO, Sh-Ctrl + Nec-1, Sh-CHMP4C + DMSO or Sh-CHMP4C + Nec-1 groups. (D-F) The expressions of RIPK1, RIPK3, MLKL and their phosphorylated proteins in tumour tissues (Kruskal-Wallis test). (G) ICH was performed to assess the expression of CHMP4C, Ki67, and p-MLKL in xenografted tumor tissues. *P < 0.05; **P < 0.01; ***P < 0.001. Data are presented as mean \pm SD.

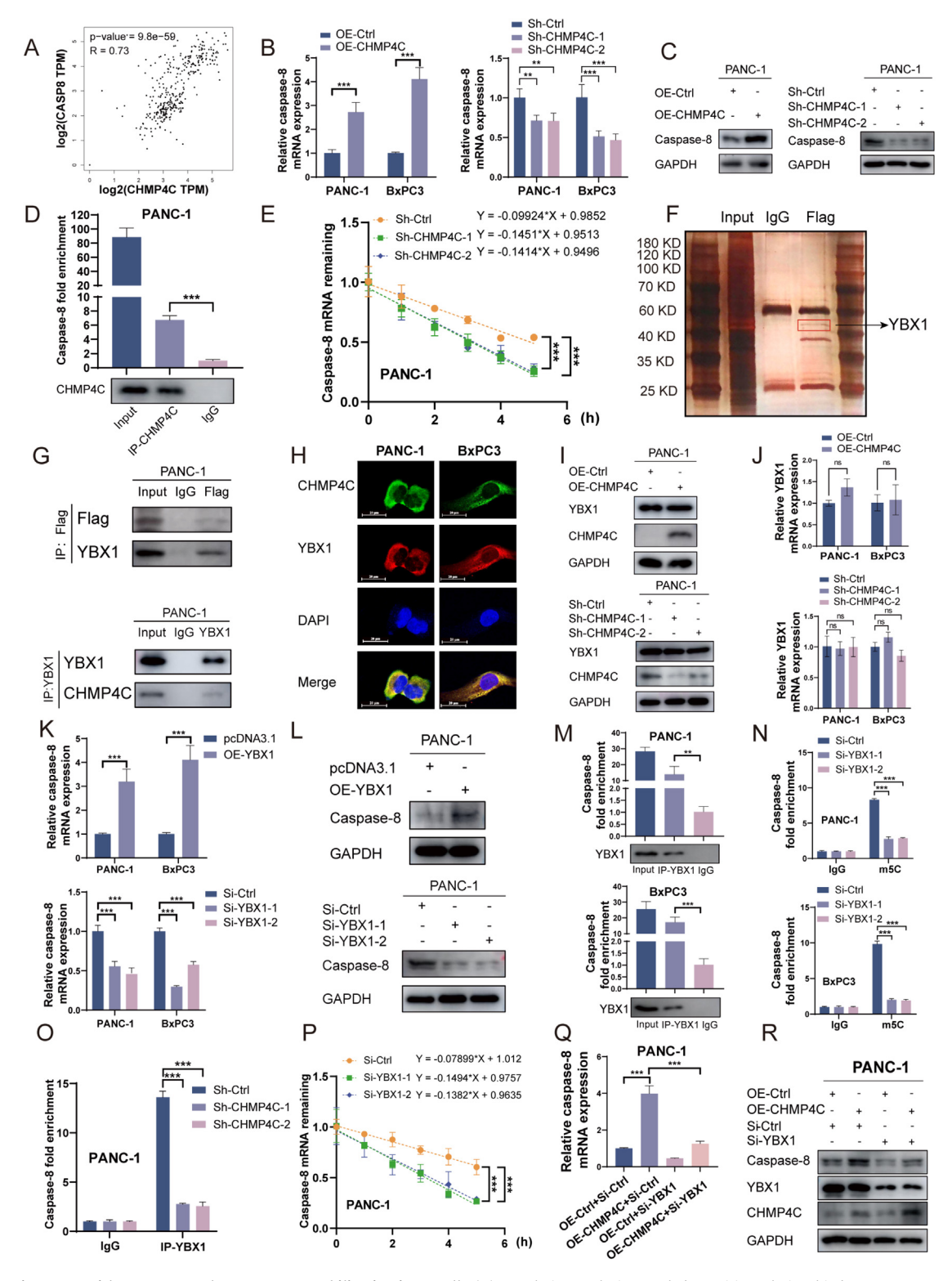


Fig. 5. CHMP4C interacts with YBX1 to regulate caspase-8 stabilization in PC cells. (A) Correlation analysis revealed a positive relationship between CHMP4C and caspase-8 mRNA levels (Pearson's analysis). (B, C) RT-qPCR and western blotting analysis showed the effect of CHMP4C on caspase-8 (Mann-Whitney *U* test and Kruskal-Wallis test). (D) RP assays showed that CHMP4C could bind to caspase-8 mRNA in PANC-1 cells. (E) RNA stability analysis showed that the half-life of caspase-8 mRNA was shortened in CHMP4C knockdown PANC-1 cells compared to control cells (Kruskal-Wallis test). (F) The proteins co-immunoprecipitated from CHMP4C-overexpressing PANC-1 cells were separated by SDS-PAGE, followed by silver staining to visualize the protein bands on the gel. (G) IP assays showed interactions between Flag-CHMP4C and YBX1 in CHMP4C-overexpressing PANC-1 cells. (H) IF staining showed that CHMP4C was colocalized with YBX1 in PANC-1 and BxPC3 cells. (I, J) Western blotting analysis and RT-qPCR results showed the effect of CHMP4C on YBX1 expression (Mann-Whitney *U* test and Kruskal-Wallis test). (K, L) RT-qPCR and western blotting analysis showed the effect of YBX1 on caspase-8 (Mann-Whitney *U* test and Kruskal-Wallis test). (M) RIP assays showed that YBX1 could bind to caspase-8 mRNA in PANC-1 cells (Mann-Whitney *U* test). (N) MeRIP-qPCR revealed the relative m⁵C modification levels of caspase-8 mRNA after knockdown of YBX1 (Kruskal-Wallis test). (O) Significant reduction of YBX1 binding to caspase-8 when CHMP4C was silenced in PANC-1 cells (Kruskal-Wallis test). (P) Effect of YBX1 knockdown on caspase-8 mRNA half-life in PANC-1 cells by RNA stability analysis (Kruskal-Wallis test). (Q, R) Knockdown of YBX1 reduced elevated caspase-8 mRNA and protein levels induced by CHMP4C upregulation in PANC-1 cells (Kruskal-Wallis test). "P < 0.005; "**P < 0.001: "***P < 0.001. Data are presented as mean ± SD.

mental Fig. S3C). To investigate the potential mechanism of caspase-8 regulation by CHMP4C, CO-IP and MS analysis were conducted to identify interacting proteins associated with CHMP4C. The results of silver staining showed differential imprints when comparing IP-Flag and IgG groups (Fig. 5F). Among the differential proteins by MS analysis (Supplemental Table 4), Y-box binding protein 1 (YBX1) is a cold shock protein that can bind to RNA, is mainly localized in the cytoplasm, and regulates the stability of RNA by 5-methylcytosine (m⁵C) modification [36,37]. Co-IP further identified that YBX1 interacted with Flag-tagged CHMP4C (Fig. 5G and Supplemental Fig. S3D) and their co-localization was demonstrated through confocal fluorescence microscopy (Fig. 5H). Further validation by western blotting and RT-qPCR revealed that YBX1 levels remained unchanged in the CHMPC4 upregulated PC cells and that knockdown of CHMPC4 did not affect YBX1 mRNA and protein expression, suggesting that YBX1 is a binding chaperone for CHMPC4 rather than a downstream target (Fig. 51. I and Supplemental Fig. S3E). In addition, the pattern of CHMP4C and YBX1 protein docking and the amino acid residues involved in putative binding were predicted using Alpha Fold3 and Pymol software (Supplemental Fig. S3F). Then, we transfected a YBX1 plasmid or siRNA into PC cells. Western blotting and RT-qPCR were used to detect transfection efficiency (Supplemental Fig. S4A and B). Based on analysis of the TCGA and GTEx databases, YBX1 had a positive correlation with caspase-8 mRNA expression in PC (Supplemental Fig. S4C). Consistent with our hypothesis, we observed that upregulation of YBX1 resulted in increased caspase-8 mRNA and protein levels. In contrast, silencing of YBX1 inhibited caspase-8 expression, leading to increased phosphorylation levels of the RIPK1/RIPK3/MLKL pathway, which further suggested that CHMPC4 and YBX1 interact synergistically (Fig. 5K, L, Supplemental Fig. S4D and E). RIP assays further indicated that YBX1 bound to caspase-8 mRNA (Fig. 5M). Subsequent experiments explored whether caspase-8 was regulated by the CHMP4C/YBX1 complex in a m⁵C-dependent manner. MeRIP assays using m⁵C antibodies revealed that YBX1 and CHMP4C knockdown resulted in significant down-regulation of caspase-8 mRNA m⁵C modification in PC cells (Fig. 5N and Supplemental Fig. S4F). Furthermore, silencing of CHMP4C significantly reduced the binding of YBX1 protein to caspase-8 mRNA (Fig. 50 and Supplemental Fig. S4G). Further investigation revealed that YBX1 depletion reduced the half-life of caspase-8 mRNA in PC cells (Fig. 5P and Supplemental Fig. S4H). In addition, silencing YBX1 led to the reduction of caspase-8 mRNA and protein in CHMP4Coverexpressing PANC-1 and BxPC3 cells (Fig. 5Q, R, Supplemental Fig. S4I and J), suggesting that YBX1 is required for CHMP4Cmediated caspase-8 mRNA stabilization. Collectively, these data suggest that CHMP4C upregulates the expression of caspase-8 by increasing the stability of caspase-8 mRNA in a YBX1-dependent manner in PC cells.

CHMP4C increases extracellular exocytosis of p-MLKL to inhibit necroptosis of PC cells

Given that CHMP4C is one of the ESCRT-III complexes, we explored whether CHMP4C affects PC cell EVs secretion. GSEA performed using the PAAD gene pool in the TCGA database revealed that genes regulated by high CHMP4C expression were primarily concentrated in the late endosome to vacuole transport and multivesicular body sorting pathway (Supplemental Fig. S5A). Furthermore, we purified EVs from cell culture supernatants of PC cells and their morphological characteristics are illustrated in Fig. 6A. NTA analysis further confirmed an average particle size of approximately 102.7 and 121.8 nm, and that the number of EVs was significantly increased in the CHMP4C overexpression group (Fig. 6B). To determine whether CHMP4C expression was different in the EVs

derived from stably transfected PANC-1 cells, we conducted a western blot analysis. As expected, the levels of CHMP4C and the classical EVs markers CD63, Alix and TSG101 were higher in EVs derived from PANC-1 cells overexpressing CHMP4C compared to controls. Meanwhile, the knockdown group exhibited the opposite result and no detectable expression of the negative EVs marker calnexin (Fig. 6C). We further identified that p-MLKL and MLKL expression were elevated in EVs derived from PANC-1 cells overexpressing CHMP4C (OE-EVs) relative to controls (Ctrl-EVs), which was attenuated by treatment with exosome inhibitor GW4869 (Fig. 6**D**). Following treatment with GW4869, there was a notable increase in the levels of both intracellular MLKL and p-MLKL (Fig. 6E). In addition, GW4869 pretreatment sensitized PC cells to TSZ-induced necroptosis compared to the DMSO-treated group (Fig. 6F, G and Supplemental Fig. S5B), which suggested that CHMP4C may further enhance its negative regulation of necroptosis by mediating the efflux of p-MLKL through EVs. In summary, CHMP4C may mediate the extracellular release of p-MLKL via EVs to inhibit PC cells necroptosis.

CHMP4C within EVs mediated intercellular communication contributes to PC progression

To explore the role of EVs-packaged CHMP4C within the tumor microenvironment, conducted an in-depth analysis of single cell data on the GSE111672 dataset and identified that the expression of CHMP4C was primarily observed in tumor cells, pancreatic ductal cells, Tprolif, and MCs (Supplemental Fig. S6A). As an vital part of the tumor microenvironment, MCs contribute to promoting tumor growth by releasing a variety of inflammatory mediators [38]. The initial objective was to analyze the effect of CM from PCs on the migration of MCs. As shown in Fig. 7A, CM of PANC-1 cells overexpressing CHMP4C significantly promoted the chemotactic migration of HMC-1. Western blotting and RT-qPCR results further verified that CHMP4C overexpression was significantly associated with elevated mRNA and protein levels of CCL2, CCL5, and SCF, while knockdown of CHMP4C inhibited their expression (Fig. 7B and C). These results suggest that CHMP4C may promote HMC-1 recruitment through the secretion of specific chemokines by PC tumor cells. Based on these findings, we postulate that intercellular communication between PC cells and mast cells play a crucial role in the malignant progression of PC.

To explore the function of EVs-packaged CHMP4C in cellular communication, we tracked the internalization of pkh67-labeled EVs by HMC-1 (Fig. 7**D**). Following the uptake of EVs by HMC-1 cells, an increase in CHMP4C protein levels was observed (Fig. 7**E**). To determine whether EVs-packaged CHMP4C regulated PC progression in an MC-dependent manner, the levels of specific cytokines in HMC-1 supernatants were assessed in the presence of PC-EVs. The results of RT-qPCR, ELISA and western blotting assays revealed that VEGFA, IL-6, TGF- β and IL-8 were all significantly elevated in the supernatant of HMC-1 treated with OE-EVs compared to Ctrl-EVs and the control group (Fig. 7**I**, **J** and Supplemental Fig. S6C). The results of the CCK8 and clone formation assays further indicated that the supernatant of HMC-1 cells stimulated by PC-EVs promoted the growth of PC cells, and the results were more significant after OE-EVs stimulation (Fig. 7**K** and L).

The clinical significance of CHMP4C in human PC tissues

To validate the function of CHMP4C and assess its clinical significance, we analyzed the expression levels of CHMP4C, p-MLKL and MCs marker (CD117) on a PC tissue microarray using multiplex immunofluorescence staining. A total of 83 pairs of cases, including PAAD and normal tissues, were used for analysis, excluding cases with inadequate fixation, poor handling, or insufficient clinical

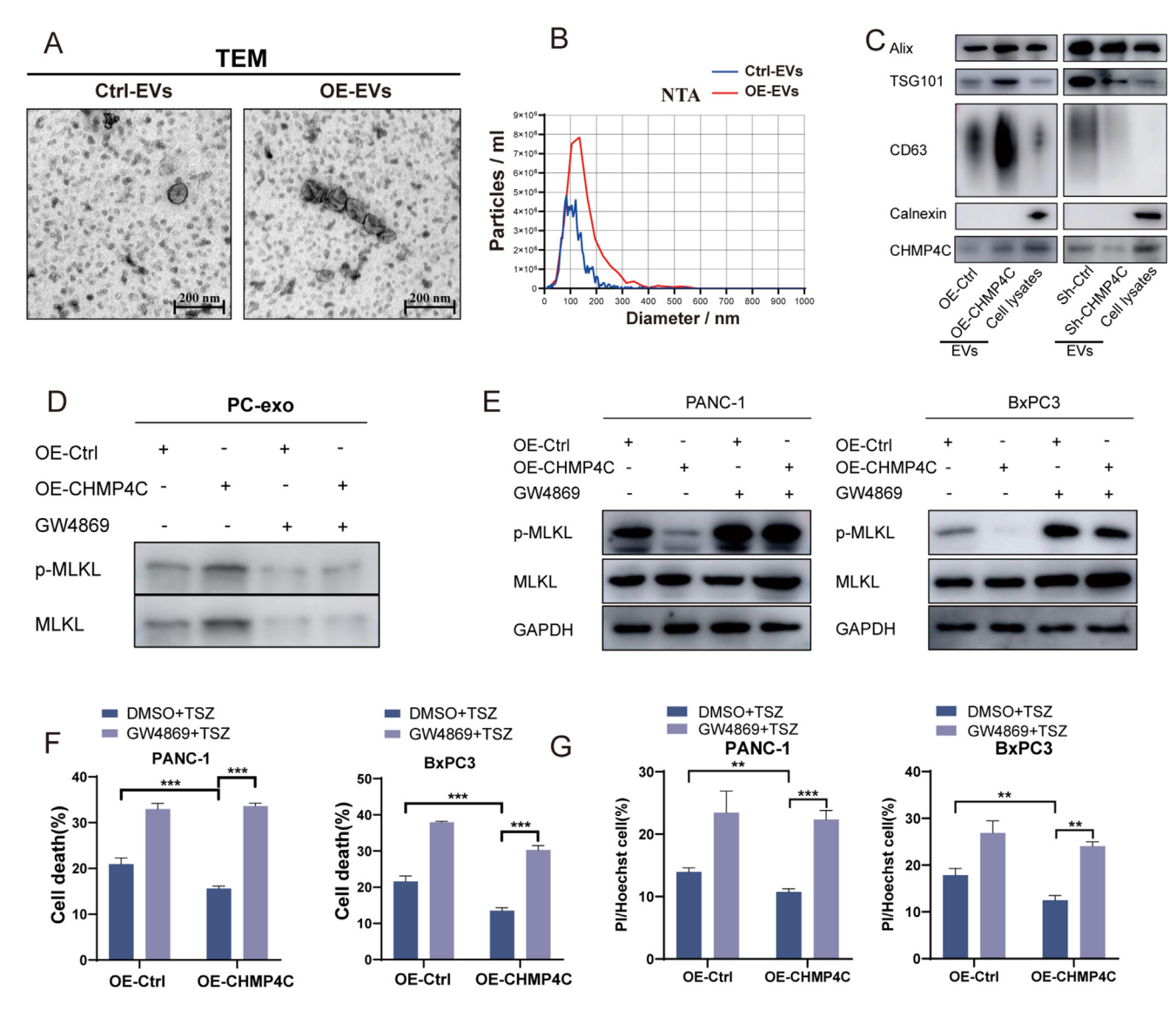


Fig. 6. CHMP4C increases efflux of p-MLKL via EVs to inhibit necroptosis of PC cells. (A) TEM of PC-derived EVs (scale bar = 200 nm). (B) NTA of PC-derived EVs. (C) Western blotting analysis showed the expression of common EVs biomarkers and CHMP4C in EVs derived from stably transfected PANC-1 cells. (D) Western blotting analysis shows MLKL and p-MLKL expression in EVs after treatment with GW4869 (20 μ M) for 24 h. (E) The expressions of MLKL and p-MLKL in control and CHMP4C-overexpressing PC cells after treatment with GW4869 (20 μ M) for 24 h were detected by western blotting analysis. (F) Cell viability of control and CHMP4C-overexpressing PANC-1 or BxPC3 cells after treatment with TSZ in the absence or presence of GW4869 (20 μ M) for 24 h. (G) Hoechst 33342/Pl double staining showed Pl uptake of control and CHMP4C-overexpressing PANC-1/BxPC3 cells after treatment with TSZ in the absence or presence of GW4869 (20 μ M) for 24 h. Kruskal-Wallis test, *P < 0.05; **P < 0.001. Data are presented as mean \pm SD.

data. As shown in Fig. 8A, CHMP4C was significantly elevated in PC tissues compared to normal controls. And, 63.9 % (53/83) cases showed upregulated in tumor tissues (Fig. 8B).

Correlation analysis revealed a significant negative relationship between the levels of CHMP4C and p-MLKL proteins (Fig. 8C). Moreover, p-MLKL in the CHMP4C overexpression group was mainly distributed in the cytoplasm, while p-MLKL in the low-level CHMP4C group was localized in the cell membrane (Supplemental Fig. S7A). Consistent with the chemotactic migration experiment, tumor tissues overexpressing CHMP4C were accompanied by increased MCs infiltration (Fig. 8D and Supplemental Fig. S7B). Contrary to the lack expression of CHMP4C in MC line, HMC-1, we observed the expression of CHMP4C in MCs of PC tissues, thereby suggesting the CHMP4C expressed in MCs cell might mainly come from the EVs released from PC cells (Fig. 8E).

The relationship between CHMP4C expression and clinicopathologic characteristics were shown in Table 1. PC patients with

poor differentiation or multiple lesions had high expression of CHMP4C. The Kaplan-Meier survival analysis indicated that patients exhibiting elevated levels of CHMP4C had poorer OS (Fig. 8F). Similarly, additional analysis of data from the TCGA and GTEx databases confirmed that high CHMP4C expression correlates with unfavorable patient prognosis (Supplemental Fig. S7C). Additionally, an increase in the infiltration of MCs suggested lower survival (Fig. 8G).

Discussion

The delineation of specific gene expression signatures associated with PC enhances comprehension of the molecular mechanisms underlying its pathogenesis and progression. In the present study, we describe novel evidence demonstrating that CHMP4C is upregulated in PC tissues resulting in its promotion of tumorigenesis. We revealed a crucial role for CHMP4C in reg-

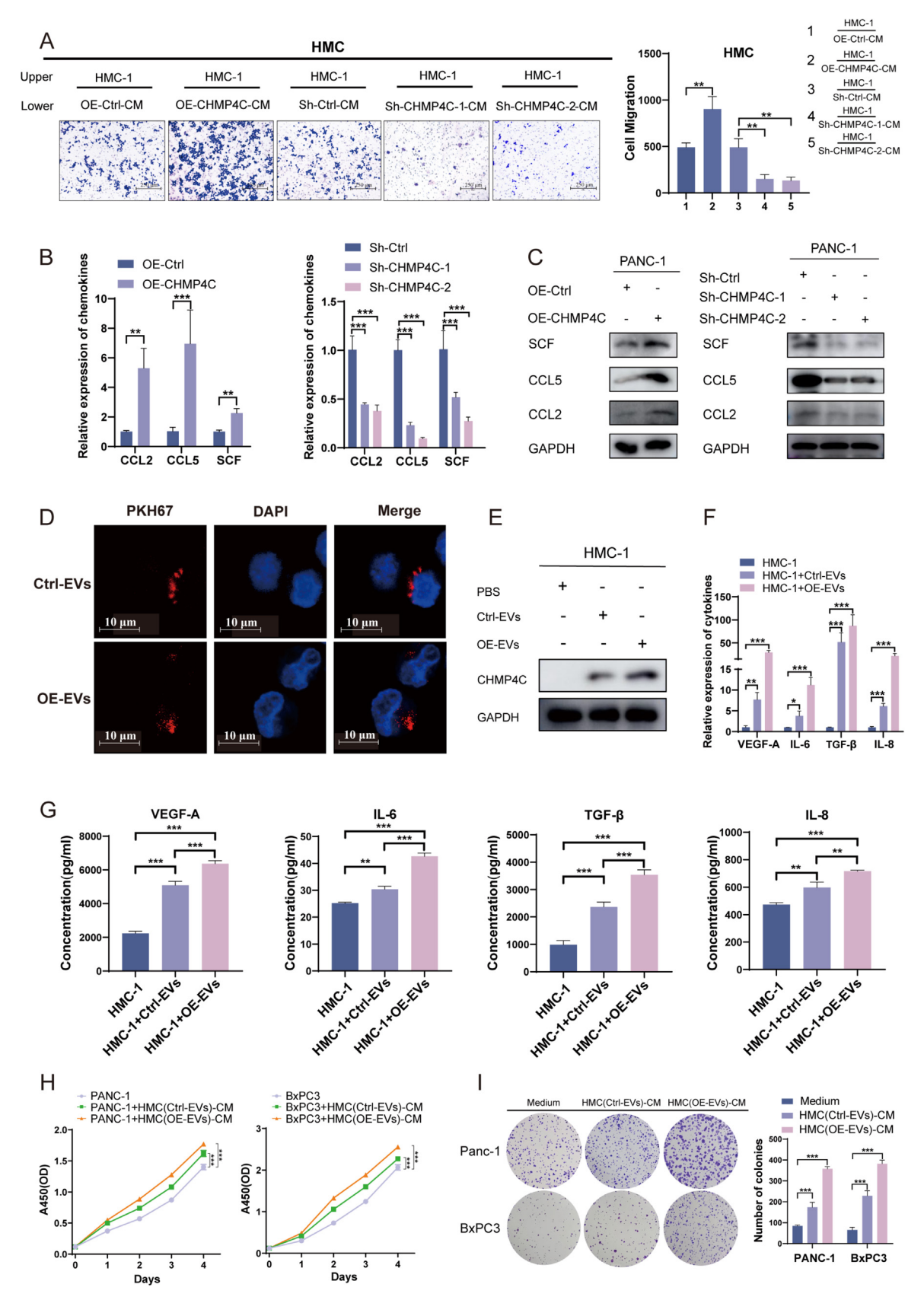


Fig. 7. Extracellular vesiclese-packaged CHMP4C-mediated intercellular communication contributes to PC progression. (A) Effect of PC-CM on mast cell migration. (B) RT-qPCR results showed the effect of CHMP4C on CCL2, CCL5 and SCF mRNA. (C) The protein level of the CCL2, CCL5 and SCF were analyzed by western blotting. (D) The uptake of PKH67-labeled PC-exo in HMC-1 cells was assayed by confocal microscopy. Scale bar = 10 μm. (E) Western blotting analysis results showed CHMP4C expression in HMC-1 cells co-cultured with PC-exo for 48 h. (F) VEGFA, IL-6, TGF-β and IL-8 mRNA expression in PC-exo-treated HMC-1 were measured with RT-qPCR. (G) The expression levels of VEGFA, IL-6, TGF-β, and IL-8 in the supernatants of PC-exo-treated HMC-1 cells were detected by ELISA. (H, I) CCK8 and colony formation assays represented effects of supernatants of HMC-1 on the proliferation of PC cells. Kruskal-Wallis test, *P < 0.05; **P < 0.01; ***P < 0.001. Data are presented as mean ± SD.

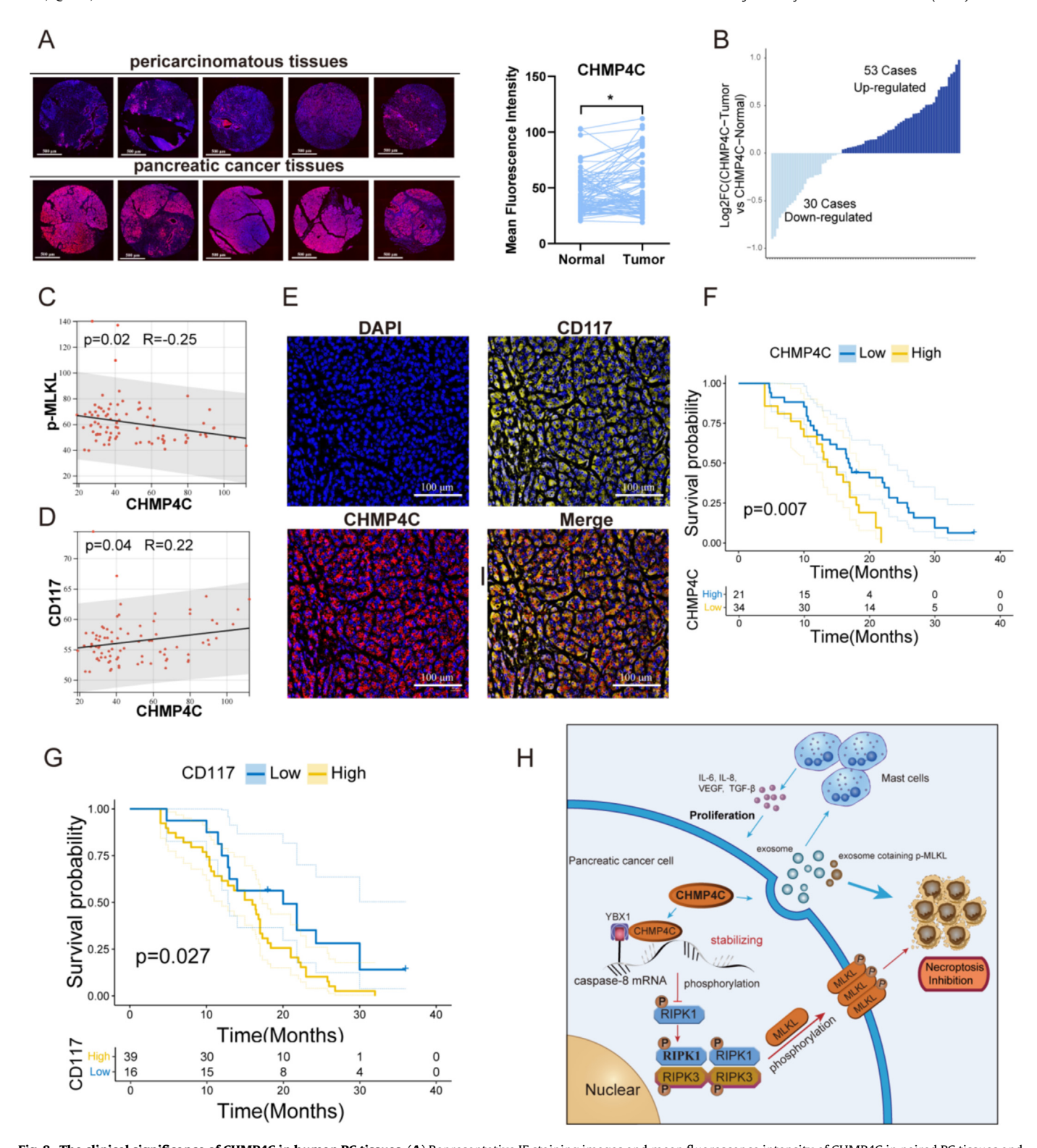


Fig. 8. The clinical significance of CHMP4C in human PC tissues. (A) Representative IF staining images and mean fluorescence intensity of CHMP4C in paired PC tissues and adjacent non-tumor tissues from tissue microarry. Scale bar = 500 μm, (paired Student *t* test). (B) Bar graph showing CHMP4C expression in 83 pairs of tissues. (C) Correlation analysis of the fluorescence intensity of CHMP4C and p-MLKL in PC tissues (Pearson's analysis). (D) Correlation analysis of the fluorescence intensity of CHMP4C and CD117 in PC tissues (Pearson's analysis). (E) IF staining of PC tissues showed the expression of CHMP4C in mast cells. Scale bar = 100 μm. (F) Kaplan-Meier survival curves for overall survival based on CHMP4C expression levels in PC tissues with CHMP4C upregulation (log-rank test). (G) Kaplan-Meier survival curves for overall survival based on CD117 expression levels in PC tissues with CHMP4C upregulation (log-rank test). (H) The schematic figure illustrates the mechanism by which CHMP4C inhibits necroptosis and promotes EVs secretion to facilitate pancreatic cancer progression.

ulating necroptosis *in vitro* and *in vivo*. Interestingly, CHMP4C also contributes to the formation of EVs to further inhibit necroptosis. Additionally, EVs-packaged CHMP4C derived from PC cells was shown to influence the migration of mast cells

within the immune microenvironment, leading to the secretion of proinflammatory factors that further promote PC growth. Finally, our results showed CHMP4C could be as a prognostic predictor for PC.

Table 1Correlation between CHMP4C expressions and clinicopathological parameters.

Clinical variables	Cases	CHMP4C Expression		χ2	P value
		Low (41)	High (42)		
Gender					
Female	51	26 (51.0 %)	25 (49.0 %)	0.133	0.716
Male	32	15 (46.9 %)	17 (53.1 %)		
Age (years)					
≤60	40	20 (50.0 %)	20 (50.0 %)	0.011	0.916
> 60	43	21 (48.8 %)	22 (51.2 %)		
Tumor size					
< 4 cm	43	22 (51.2 %)	21 (48.8 %)	0.111	0.739
≥ 4 cm	40	19 (47.5 %)	21 (52.5 %)		
Differentiation					
Well-Moderate	47	29 (59.6 %)	19 (40.4 %)	4.490	0.034*
Poor	36	13 (36.1 %)	23 (63.9 %)		
T stage					
T1-T2	42	19 (45.2 %)	23 (54.8 %)	0.589	0.443
T3-T4	41	22 (53.7 %)	19 (46.3 %)		
Lymph nodes metastasis					
No	31	15 (48.4 %)	16 (51.6 %)	0.020	0.887
Yes	52	26 (50.0 %)	26 (50.0 %)		
Distant metastasis					
No	61	28 (45.9 %)	33 (54.1 %)	1.125	0.289
Yes	22	13 (59.1 %)	9 (40.9 %)		
TNM stage					
I-II	50	22 (44.0 %)	28 (56.0 %)	1.466	0.226
III-IV	33	19 (57.6 %)	14 (42.4 %)		
Lesions		• •	, ,		
Single lesion	44	29 (65.9 %)	15 (34.1 %)	5.083	0.024*
Multiple lesions	13	4 (30.8 %)	9 (69.2 %)		

P value was estimated by a $\chi 2$ test. * represents P values smaller than 0.05.

Tumor cells that resist apoptosis might become more susceptible to necroptosis when specific components of the apoptotic pathway are inhibited. Consequently, necroptosis may be regarded as a viable alternative mechanism of cell death to circumvent resistance to apoptosis [39]. Chen et al. [40] reported reducing CHMP4C clearly suppressed the proliferation and metastasis capabilities of PC cells. However, the underlying mechanism of CHMP4C in PC is still unclear. In the present study, our findings demonstrated that CHMP4C promoted PC cells growth through suppression of necroptosis in both in vivo and in vitro settings. And, knockdown of CHMP4C induced the RIPK1/RIPK3/MLKL necroptosis of PC cells and inhibited the tumor proliferation. These findings were similar to the research studied by Lin et al. that TRAF6 promoted colorectal tumor growth primarily through inhibiting necroptosis [28]. Thus, targeting CHMP4C may be a useful therapeutic strategy for inducing necroptosis of PC.

Caspase-8 plays a crucial role in regulating both necroptosis and apoptosis by cleaving or inactivating RIPK1 and RIPK3, triggering the pro-apoptotic caspase cascade [41]. In the absence of functional caspase-8, cells switch from the apoptosis to the necroptosis [42]. Mechanistically, caspase-8 deficiency triggers autophosphorylation of RIPK1 at Ser166 and facilitates its interaction with RIPK3 through the RIP homology interaction motif (RHIM) structural domain, resulting in the phosphorylation of RIPK3 at Ser358. Subsequently, activated RIPK3 promotes the recruitment and phosphorylation of MLKL to form the necrosome (complex IIb) [43,44]. Our findings demonstrated that elevated levels of CHMP4C correlate with upregulation of caspase-8, whereas decreased levels of CHMP4C had the opposite effect. Subsequent investigation revealed that the modulation of caspase-8 mRNA stability by CHMP4C is contingent upon the presence of YBX1. Previous studies have demonstrated that YBX1 functions as an RNA binding protein capable of serving as an m⁵C reader, it is a critical component in the regulation of mRNA stability facilitated by the RNA methyltransferase NSUN2 [36,45]. Similarly, our findings revealed that YBX1 stabilized caspase-8 mRNA in m⁵C modification-dependent manner, further underscoring its central role in mRNA stability regulation. Additionally, the depletion of CHMP4C hindered the interaction between YBX1 and caspase-8 mRNA, consequently impeding the regulatory role of YBX1 and resulting in reduced m⁵C methylation and stability of caspase-8 mRNA. For the first time, the present study has demonstrated, that CHMP4C interacts with YBX1 to stabilize caspase-8 mRNA through m⁵C modification, subsequently resulting in the inhibition of the RIPK1/RIPK3/MLKL signaling cascade.

Recent studies have reported that extracellular vesicles transport various molecules from cancer cells, many of which are tumor suppressing molecules that can be selectively encapsulated into the extracellular vesicles and released, thereby enhancing the malignant phenotype of cancer cells [46]. MLKL serves as the effector of necroptosis, and oligomeric MLKL exhibits movement and localization to the cell membrane, where it helps to form holes in the cell membrane by binding to phosphatidylinositol phosphate, resulting in the disruption of membrane integrity [47]. Additionally, MLKL interacts with ion channels or potentiates the assembly of cation channels, enhancing Ca²⁺, Na⁺, and K⁺ influx and increasing cell membrane permeability, ultimately culminating in necroptosis [48]. In present study, we uncovered that CHMP4C promoted EVs release, increased the efflux of p-MLKL, and further inhibited necroptosis. After treatment with exosome inhibitor GW4869, the expression of intracellular MLKL and p-MLKL were restored and necroptosis was more likely to occur. An earlier study is reported that ESCRT-III is not only involved in MVBs formation, but also participates in the repair of plasma membrane damage induced by MLKL activation during necroptosis [49]. As CHMP4C is one of the components of ESCRT-III, we hypothesize that the EVs play a crucial role in CHMP4C –regulated necroptosis.

Our finding suggests that CHMP4C in infiltrating mast cells might originate from EVs secreted by PC cells. Meanwhile, our results showed that tumor tissues with high levels of expression of CHMP4C display greater numbers of infiltrating MCs, indicating the significance of mast cells in the immune microenvironment of

PC with elevated CHMP4C expression. Bergot et al. [50] found that CCL2 and CCL5 could recruit MCs and thus contributed to an immunosuppressive environment. Meanwhile. CCL5-mediated MCs infiltration promoted the progression of clear cell renal cell carcinoma and was associated with poor patient prognosis [51]. Together with CCL2 and CCL5, continuous stimulation by SCF promoted the accumulation of MCs and facilitated chronic inflammation towards cancer [52]. Similarly, our study further supports this by demonstrating that CHMP4C increased the expression and secretion of CCL2, CCL5 and SCF to recruit MCs for infiltration. Moreover, we confirmed MCs could release VEGF, TGF-β, IL-6, and IL-8 after phagocytosing EVs, promoting PC cell growth, similar to some findings in other cancers [52–54]. Currently, there is limited research regarding the relationship between necroptosis and immune microenvironment in PC. A recent study reported MLKL-driven necroptosis recruited and activated macrophage. and facilitates PC metastasis by evading immune surveillance [55], while our results realized CHMP4C induced necroptosis inhibition was association with recruitment and activation of MCs, which contributed to PC progression. Therefore, the necroptosis of PC cells may affect the immune microenvironment in different

Conclusion

This study indicates that CHMP4C and its downstream signaling molecules play a key role in inhibiting necroptosis and facilitating subsequent PC progression. The mechanism by which CHMP4C regulates necroptosis may be regarded as follows: on the one hand, CHMP4C enhances the stability of caspase-8 mRNA by binding to YBX1, inhibiting the phosphorylation of the RIPK1/RIPK3/MLKL pathway, antagonizing necroptosis and promoting the progression of pancreatic cancer; on the other hand, CHMP4C further enhances its negative regulatory effect on necroptosis by mediating the excretion of p-MLKL from extracellular vesicles. In addition, the EVs-packaged CHMP4C derived from PC cells can modulate the recruitment of MCs in the immune microenvironment and stimulate MCs to release proinflammatory factors that in turn promote the growth of PC cells. These mechanisms are summarized in Fig. 8H. Accordingly, our study provides novel insights into the function of CHMP4C and the mechanisms underlying necroptosis. Moreover, these findings highlight that CHMP4C has potential as a biomarker and therapeutic target in PC.

Compliance with ethics requirements

The animal study was approved by the Animal Care and Use Committee of Qilu Hospital of Shandong University (Certification No. DWLL-202400053). The clinical samples and data used in this study were approved by the Ethics Committee of Qilu Hospital of Shandong University (Certification No. KYLL-202207-005) and the Ethics Committee of Shanghai Outdo Biotech Company (Certification No. YB M-05-02).

Availability of data and materials

The data and materials analyzed in this study are accessible from the corresponding author upon reasonable request.

Funding

This research received funding from the National Natural Science Foundation of China (82172339), Major Scientific and Technological Innovation Project of Shandong Province (2021CXGC011105), and Taishan scholar program of Shandong Province (tsqn202306346).

Declaration of competing interest

The authors declare that they have no known competing financial interests or personal relationships that could have appeared to influence the work reported in this paper.

Appendix A. Supplementary material

Supplementary data to this article can be found online at https://doi.org/10.1016/j.jare.2025.01.040.

References

- [1] Siegel RL, Giaquinto AN, Jemal A. Cancer statistics, 2024. CA Cancer J Clin 2024;74(1):12–49.
- [2] Mizrahi JD, Surana R, Valle JW, Shroff RT. Pancreatic cancer. Lancet 2020;395 (10242):2008–20.
- [3] Park W, Chawla A, O'Reilly EM. Pancreatic cancer: a review. JAMA 2021;326 (9):851–62.
- [4] Schnelldorfer T, Adams DB, Warshaw AL, Lillemoe KD, Sarr MG. Forgotten pioneers of pancreatic surgery: beyond the favorite few. Ann Surg 2008;247 (1):191–202.
- [5] Tempero MA, Malafa MP, Al-Hawary M, Behrman SW, Benson AB, Cardin DB, et al. Pancreatic adenocarcinoma, version 2.2021, NCCN clinical practice guidelines in oncology. J Natl Compr Canc Netw 2021;19(4):439–57.
- [6] Vasan N, Baselga J, Hyman DM. A view on drug resistance in cancer. Nature 2019;575(7782):299–309.
- [7] Seo J, Nam YW, Kim S, Oh DB, Song J. Necroptosis molecular mechanisms: recent findings regarding novel necroptosis regulators. Exp Mol Med 2021;53 (6):1007-17
- [8] Gong Y, Fan Z, Luo G, Yang C, Huang Q, Fan K, et al. The role of necroptosis in cancer biology and therapy. Mol Cancer 2019;18(1):100.
- [9] Hannes S, Abhari BA, Fulda S. Smac mimetic triggers necroptosis in pancreatic carcinoma cells when caspase activation is blocked. Cancer Lett 2016;380 (1):31–8.
- [10] Meier P, Legrand AJ, Adam D, Silke J. Immunogenic cell death in cancer: targeting necroptosis to induce antitumour immunity. Nat Rev Cancer 2024;24 (5):299–315.
- [11] Zhao Q, Zheng Y, Lv X, Gong J, Yang L. IMB5036 inhibits human pancreatic cancer growth primarily through activating necroptosis. Basic Clin Pharmacol Toxicol 2022;130(3):375–84.
- [12] Seifert L, Werba G, Tiwari S, Giao Ly NN, Alothman S, Alqunaibit D, et al. The necrosome promotes pancreatic oncogenesis via CXCL1 and Mincle-induced immune suppression. Nature 2016;532(7598):245–9.
- [13] Chen L, Zhang X, Zhang Q, Zhang T, Xie J, Wei W, et al. A necroptosis related prognostic model of pancreatic cancer based on single cell sequencing analysis and transcriptome analysis. Front Immunol 2022;13:1022420.
- [14] Liu H, Li Z, Zhang L, Zhang M, Liu S, Wang J, et al. Necroptosis-Related Prognostic Model for Pancreatic Carcinoma Reveals Its Invasion and Metastasis Potential through Hybrid EMT and Immune Escape. Biomedicines 2023;11(6).
- [15] Colombo M, Raposo G, Théry C. Biogenesis, secretion, and intercellular interactions of exosomes and other extracellular vesicles. Annu Rev Cell Dev Biol 2014:30:255–89.
- [16] Sun W, Ren Y, Lu Z, Zhao X. The potential roles of exosomes in pancreatic cancer initiation and metastasis. Mol Cancer 2020;19(1):135.
- [17] Takahashi A, Okada R, Nagao K, Kawamata Y, Hanyu A, Yoshimoto S, et al. Exosomes maintain cellular homeostasis by excreting harmful DNA from cells. Nat Commun 2017;8:15287.
- [18] Yoon S, Kovalenko A, Bogdanov K, Wallach D. MLKL, the Protein that mediates necroptosis, also regulates endosomal trafficking and extracellular vesicle generation. Immunity 2017;47(1):51–65.e7.
- [19] Peng L, Wang Y, Yang B, Qin Q, Song E, Song Y. Polychlorinated biphenyl quinone regulates MLKL phosphorylation that stimulates exosome biogenesis and secretion via a short negative feedback loop. Environ Pollut 2021;274:115606.
- [20] Petsalaki E, Dandoulaki M, Zachos G. The ESCRT protein Chmp4c regulates mitotic spindle checkpoint signaling. J Cell Biol 2018;217(3):861–76.
- [21] Zhang H, Liu D, Qin Z, Yi B, Zhu L, Xu S, et al. CHMP4C as a novel marker regulates prostate cancer progression through cycle pathways and contributes to immunotherapy. Front Oncol 2023;13:1170397.
- [22] Liu B, Guo S, Li GH, Liu Y, Liu XZ, Yue JB, et al. CHMP4C regulates lung squamous carcinogenesis and progression through cell cycle pathway. J Thorac Dis 2021;13(8):4762–74.
- [23] Lin SL, Wang M, Cao QQ, Li Q. Chromatin modified protein 4C (CHMP4C) facilitates the malignant development of cervical cancer cells. FEBS Open Bio 2020;10(7):1295–303.
- [24] Honegger A, Leitz J, Bulkescher J, Hoppe-Seyler K, Hoppe-Seyler F. Silencing of human papillomavirus (HPV) E6/E7 oncogene expression affects both the

- contents and the amounts of extracellular microvesicles released from HPV-positive cancer cells. Int J Cancer 2013;133(7):1631–42.
- [25] Porcelli L, Iacobazzi RM, Di Fonte R, Serratì S, Intini A, Solimando AG, et al. CAFs and TGF-β Signaling Activation by Mast Cells Contribute to Resistance to Gemcitabine/Nabpaclitaxel in Pancreatic Cancer. Cancers (Basel) 2019;11(3).
- [26] Zhang X, Zhang Y, Gui X, Zhang Y, Zhang Z, Chen W, et al. Salivary Fusobacterium nucleatum serves as a potential biomarker for colorectal cancer. iScience. 2022;25(5).
- [27] Cao S, Zhou Y, Xu P, Wang Y, Yan J, Bin W, et al. Berberine metabolites exhibit triglyceride-lowering effects via activation of AMP-activated protein kinase in Hep G2 cells. J Ethnopharmacol 2013;149(2):576–82.
- [28] Lin P, Lin C, He R, Chen H, Teng Z, Yao H, et al. TRAF6 regulates the abundance of RIPK1 and inhibits the RIPK1/RIPK3/MLKL necroptosis signaling pathway and affects the progression of colorectal cancer. Cell Death Dis 2023;14(1):6.
- [29] Stribbling SM, Ryan AJ. The cell-line-derived subcutaneous tumor model in preclinical cancer research. Nat Protoc 2022;17(9):2108–28.
- [30] Dou X, Xiao Y, Shen C, Wang K, Wu T, Liu C, et al. RBFOX2 recognizes N(6)-methyladenosine to suppress transcription and block myeloid leukaemia differentiation. Nat Cell Biol 2023;25(9):1359–68.
- [31] Yu T, Zhang Q, Yu SK, Nie FQ, Zhang ML, Wang Q, et al. THOC3 interacts with YBX1 to promote lung squamous cell carcinoma progression through PFKFB4 mRNA modification. Cell Death Dis 2023;14(7):475.
- [32] Xue M, Dong L, Zhang H, Li Y, Qiu K, Zhao Z, et al. METTL16 promotes liver cancer stem cell self-renewal via controlling ribosome biogenesis and mRNA translation. J Hematol Oncol 2024;17(1):7.
- [33] Zhang M, Wang Y, Yu L, Zhang Y, Wang Y, Shang Z, et al. Fusobacterium nucleatum promotes colorectal cancer metastasis by excretion of miR-122-5p from cells via exosomes. iScience 2023;26(9):107686.
- [34] Hefele M, Stolzer I, Ruder B, He GW, Mahapatro M, Wirtz S, et al. Intestinal epithelial Caspase-8 signaling is essential to prevent necroptosis during Salmonella Typhimurium induced enteritis. Mucosal Immunol 2018;11 (4):1191–202.
- [35] Newton K, Wickliffe KE, Dugger DL, Maltzman A, Roose-Girma M, Dohse M, et al. Cleavage of RIPK1 by caspase-8 is crucial for limiting apoptosis and necroptosis. Nature 2019;574(7778):428-31.
- [36] Zou S, Huang Y, Yang Z, Zhang J, Meng M, Zhang Y, et al. NSUN2 promotes colorectal cancer progression by enhancing SKIL mRNA stabilization. Clin Transl Med 2024;14(3):e1621.
- [37] Li Y, Xue M, Deng X, Dong L, Nguyen LXT, Ren L, et al. TET2-mediated mRNA demethylation regulates leukemia stem cell homing and self-renewal. Cell Stem Cell 2023;30(8). 1072-90.e10.
- [38] Rigoni A, Colombo MP, Pucillo C. Mast cells, basophils and eosinophils: From allergy to cancer. Semin Immunol 2018;35:29–34.
- [39] Saha R, Pal R, Ganguly B, Majhi B, Dutta S. Mono-quinoxaline-induced DNA structural alteration leads to ZBP1/RIP3/MLKL-driven necroptosis in cancer cells. Eur J Med Chem 2024;270:116377.
- [40] Chen Y, Liu Y, Wang M. Identification of a Pyroptosis-Related Gene Signature and Effect of Silencing the CHMP4C and CASP4 in Pancreatic Adenocarcinoma. Int J Gen Med 2022;15:3199–213.

- [41] Khoury MK, Gupta K, Franco SR, Liu B. Necroptosis in the pathophysiology of disease. Am J Pathol 2020;190(2):272–85.
- [42] Fritsch M, Günther SD, Schwarzer R, Albert MC, Schorn F, Werthenbach JP, et al. Caspase-8 is the molecular switch for apoptosis, necroptosis and pyroptosis. Nature 2019;575(7784):683-7.
- [43] Schwarzer R, Laurien L, Pasparakis M. New insights into the regulation of apoptosis, necroptosis, and pyroptosis by receptor interacting protein kinase 1 and caspase-8. Curr Opin Cell Biol 2020;63:186-93.
- [44] Cho YS, Challa S, Moquin D, Genga R, Ray TD, Guildford M, et al. Phosphorylation-driven assembly of the RIP1-RIP3 complex regulates programmed necrosis and virus-induced inflammation. Cell 2009;137 (6):1112–23.
- [45] Liu X, Wei Q, Yang C, Zhao H, Xu J, Mobet Y, et al. RNA m(5)C modification upregulates E2F1 expression in a manner dependent on YBX1 phase separation and promotes tumor progression in ovarian cancer. Exp Mol Med 2024;56(3):600–15.
- [46] Zhao J, Cui X, Zhan Q, Zhang K, Su D, Yang S, et al. CRISPR-Cas9 library screening combined with an exosome-targeted delivery system addresses tumorigenesis/TMZ resistance in the mesenchymal subtype of glioblastoma. Theranostics 2024;14(7):2835–55.
- [47] Pasparakis M, Vandenabeele P. Necroptosis and its role in inflammation. Nature 2015;517(7534):311–20.
- [48] Xia B, Fang S, Chen X, Hu H, Chen P, Wang H, et al. MLKL forms cation channels. Cell Res 2016;26(5):517–28.
- [49] Gong YN, Guy C, Olauson H, Becker JU, Yang M, Fitzgerald P, et al. ESCRT-III acts downstream of MLKL to regulate necroptotic cell death and its consequences. Cell 2017;169(2):286–300.e16.
- [50] Bergot AS, Ford N, Leggatt GR, Wells JW, Frazer IH, Grimbaldeston MA. HPV16-E7 expression in squamous epithelium creates a local immune suppressive environment via CCL2- and CCL5- mediated recruitment of mast cells. PLoS Pathog 2014;10(10):e1004466.
- [51] Liu T, Xia Q, Zhang H, Wang Z, Yang W, Gu X, et al. CCL5-dependent mast cell infiltration into the tumor microenvironment in clear cell renal cell carcinoma patients. Aging (Albany NY) 2020;12(21):21809–36.
- [52] Molfetta R, Lecce M, Milito ND, Putro E, Pietropaolo G, Marangio C, et al. SCF and IL-33 regulate mouse mast cell phenotypic and functional plasticity supporting a pro-inflammatory microenvironment. Cell Death Dis 2023;14 (9):616.
- [53] Ammendola M, Currò G, Laface C, Zuccalà V, Memeo R, Luposella F, et al. Mast cells positive for c-Kit receptor and tryptase correlate with angiogenesis in cancerous and adjacent normal pancreatic tissue. Cells 2021;10(2).
- [54] Shi S, Ye L, Yu X, Jin K, Wu W. Focus on mast cells in the tumor microenvironment: Current knowledge and future directions. Biochim Biophys Acta Rev Cancer 2023;1878(1):188845.
- [55] Liao CY, Li G, Kang FP, Lin CF, Xie CK, Wu YD, et al. Necroptosis enhances 'don't eat me' signal and induces macrophage extracellular traps to promote pancreatic cancer liver metastasis. Nat Commun 2024;15(1):6043.